RSC Advances

PAPER

View Article Online
View Journal | View Issue

Cite this: *RSC Adv.*, 2018, **8**, 17732

Performance enhancement of PEDOT:poly(4-styrenesulfonate) actuators by using ethylene glycol†

Naohiro Terasawa * and Kinji Asaka

Received 29th March 2018
Accepted 5th May 2018

DOI: 10.1039/c8ra02714e

rsc.li/rsc-advances

This paper describes the effect of ethylene glycol on the performance of actuators with poly(3,4-ethylenedioxythiophene):poly(4-styrenesulfonate)/vapor-grown carbon fiber/ionic liquid/ethylene glycol (PEDOT:PSS/VGCF/IL/EG) structures. These devices exhibit superior strain performances compared to devices using PEDOT:PSS/VGCF/IL. EG is assumed to assist in the formation of three-dimensional conducting networks between small PEDOT:PSS domains. This is because it helps to remove insulating PSS from the surface of the PEDOT/PSS grains and facilitates the crystallization of PEDOT. Therefore, EG helps to increase the specific capacitance, strain, and maximum generated stress compared to the values obtained using a PEDOT:PSS/VGCF/IL actuator. Therefore, these new, flexible, and robust films may have significant potential for their use as actuator materials in wearable energy conversion devices. A double-layer charging kinetic model was developed to account for the oxidation and reduction reactions of PEDOT:PSS, and this model is similar to that proposed for PEDOT:PSS/VGCF/IL/EG actuators. This model was successfully applied to simulate the frequency-dependent displacement responses of the actuators.

Introduction

Conductive polymers (CPs) are well suited for applications in electrochemical capacitors because of their low cost, low environmental impact, highly conductive doped states, wide voltage windows, high storage capacities/porosities/reversibilities, and adjustable redox activities that can be tailored through chemical modification.[1–5]

Poly(3,4-ethylenedioxythiophene) (PEDOT), a polythiophene derivative, is considered to be the best CP currently available with regard to electrical conductivity, processability, and stability.[6] Thus, it is produced on a commercial scale and used in multiple applications, such as solid electrolyte capacitors, light emitting diodes, antistatic coatings, organic solar cells, and organic field-effect transistors.[6] PEDOT doped with poly(4-styrenesulfonate) (PEDOT:PSS) is one of the most important CPs because it can be dispersed in water in the form of colloidal particles. Moreover, this material has superior mechanical properties, thermal stability, and a tunable conductivity (0.1–3000 S cm^{-1}).[7,8] Therefore, it has been employed in many organic or plastic electronic/optical devices.[9–12] In other studies, PEDOT:PSS-based electrodes have been analyzed,[13–15] and the conversion of electrical to mechanical energy has been demonstrated using these devices.[16,17]

In recent years, researchers have reported on the improved conductivity of thin coatings and films by adding some organic solvents, such as ethylene glycol (EG), dimethyl sulfoxide, and sorbitol, to PEDOT/PSS aqueous dispersion.[18–21] PEDOT/PSS microfibers with conductivity as high as 467 S cm^{-1}, obtained by exploiting the solvent effect of EG, were first reported by Okuzaki *et al.*.[22] The effects of EG treatment on the electrical conductivity, structure, carrier transport properties, and mechanical properties of PEDOT/PSS microfibers have been investigated. EG helps to remove insulating PSS from the surface of PEDOT/PSS grains and helps to crystallize PEDOT, thus resulting in the formation of large numbers of highly conductive grains that improve charge carrier transport in the microfibers.

Soft materials that can convert electrical energy into mechanical energy have been studied extensively in recent years. Such materials can be used in a wide range of applications such as robotics, tactile and optical displays, prosthetic devices, medical devices, and microelectromechanical systems.[23] Low-voltage electroactive polymer (EAP)-based actuators with rapid response are particularly beneficial in this sense because they can be employed as artificial muscle-like actuators in biomedical and human-affinity applications.[24,25] We previously reported[26–28] on the first dry actuator fabricated with a "bucky gel",[29] which is a gelatinous ionic-liquid (IL)-containing single-walled carbon nanotubes (SWCNTs) at room temperature. This actuator was built with a bimorph

Inorganic Functional Material Research Institute, National Institute of Advanced Industrial Science and Technology (AIST), 1-8-31 Midorigaoka, Ikeda, Osaka 563-8577, Japan. E-mail: terasawa-naohiro@aist.go.jp

† Electronic supplementary information (ESI) available. See DOI: 10.1039/c8ra02714e

configuration, in which a polymer-supported IL electrolyte layer is placed between two polymer-supported bucky-gel electrode layers. This design facilitates rapid device operation and increases device lifespan in air at low applied voltages. Furthermore, ILs are suitable for use in quick-response actuators and devices requiring high electrochemical stability owing to their favorable characteristics, such as intrinsically low volatility, high ionic conductivity, and wide potential window.[30] In addition, we found that the electromechanical and electrochemical properties of these actuators depend on the specific IL, nanocarbon, and polymer materials employed.[28,31–34]

There are two main types of electrochemical capacitors (ECs): faradaic capacitors (FCs) and electrostatic double-layer capacitors (EDLCs). EDLCs are based on electrode materials that are not electrochemically active, which may include carbon particles. Therefore, during both charging and discharging, there are no electrochemical reactions at the electrode, although the electrode/electrolyte interface accumulates a physical charge. In contrast, FCs are able to store charge during both discharge and charge operations, and employ electrochemically active substances as electrodes, including metal oxides.[7,35,36] There are basic criteria for both types, such as the incorporation of extremely conductive electrode materials (so as to ensure high capacitance), an optimal distribution of pore sizes, and a significant surface area. In addition, it is also possible to fabricate a unit that simultaneously exhibits both FC and EDLC characteristics, with one of the two being the primary mechanism, known as a hybrid capacitor.[37]

In a previous study, we developed a film casting method to fabricate hybrid EDLC–FC PEDOT:PSS actuators that incorporate VGCFs or SWCNTs to further exploit the synergistic effects between nanotubes and PEDOT:PSS.[38,39] The strain performance of the resulting PEDOT:PSS/VGCF/IL actuators was better than that of PEDOT:PSS/SWCNT/IL and PVdF(HFP)/VGCF/IL actuators owing to the differences in their synergistic effects.

In the present study, we investigate the effect of EG on actuators with poly(3,4-ethylenedioxythiophene):poly(4-styrenesulfonate)/vapor-grown carbon fiber/ionic liquid/ethylene glycol (PEDOT:PSS/VGCF/IL/EG) structures. These devices show superior strain performances compared to the devices that use PEDOT:PSS/VGCF/IL.

Experimental

Materials

EG and PEDOT:PSS (polyion complex; 1 : 2.5 w/w) were procured from Wako Pure Chemical Industries Ltd. and Aldrich (no. 768618), respectively. The average diameter, average length, and surface area of the VGCFs (VGCF-X, Showa Denko Co., Ltd.) were 10–15 nm, 3 μm, and 270 $m^2 g^{-1}$, respectively. The ILs were 1-ethyl-3-methylimidazolium tetrafluoroborate (EMI[BF_4], Fluka) and 1-ethyl-3-methylimidazolium triflate (EMI[CF_3SO_3], Fluka) and were used as received. Fig. 1 schematically illustrates their chemical structures. Other reagents included poly(-vinylidene fluoride-*co*-hexafluoropropylene (PVdF(HFP)), Kynar Flex 2801, Arkema Chemicals, Inc.), methyl pentanone (MP, Aldrich), and propylene carbonate (PC, Aldrich) and were used as received.

Preparation of the actuator film[38]

The configuration of the EG/PEDOT:PSS/VGCF/IL actuators developed in this study is shown in Fig. 1. Typically, the EG/PEDOT:PSS/VGCF/IL electrode layer (EG 30%) comprises 9 wt% EG, 29 wt% PEDOT:PSS, 18 wt% VGCF, and 44 wt% IL. Individual layers were prepared by first mixing 24 mg EG, 80 mg PEDOT:PSS, 50 mg VGCFs, and 120 mg EMI[BF_4] or EMI[CF_3SO_3] in 9 mL H_2O, and this mixture was stirred for more than 5 h. Subsequently, 1.6 mL of the resulting gelatinous mixture was cast into a Teflon mold according to the procedure outlined above to obtain an electrode film with a thickness of 70–80 μm. Electrode layers with 3% and 0% EG were prepared using the same procedure. Gel electrolyte layers were fabricated by casting 0.3 mL of a solution containing either of the two ILs and PVdF(HFP) (100 mg each) in a mixture of 1 mL MP and 250 mg PC in a Teflon mold (2.5 cm × 2.5 cm). This was followed by solvent evaporation and the complete removal of the solvent *in*

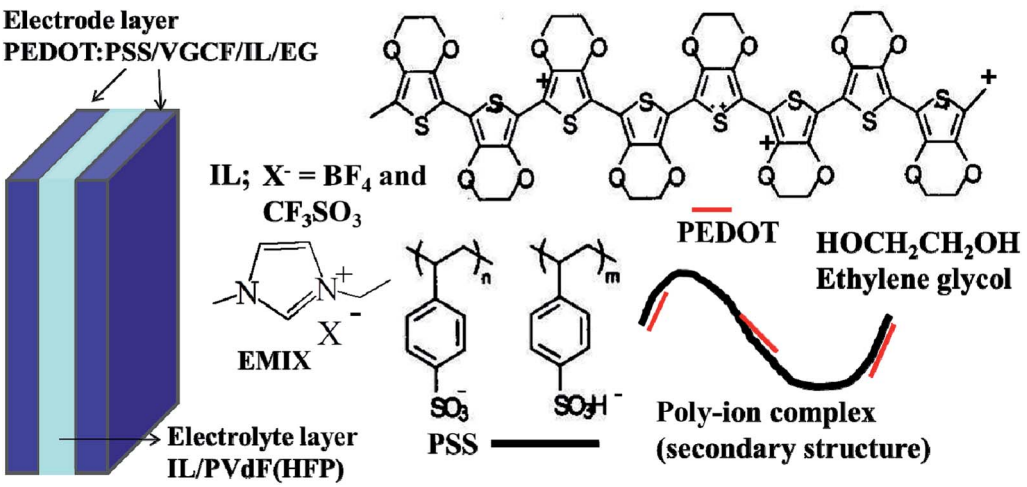

Fig. 1 Configuration of the PEDOT:PSS/VGCF/IL/EG electrode actuator, and the molecular structures of the corresponding ILs and polymers.

vacuo at 80 °C. The resulting gel electrolyte films had thicknesses of 20–30 μm. Finally, the electrode and electrolyte layers containing the same IL were hot-pressed to obtain an actuator film with a thickness of 150–175 μm. The thickness of the actuator film is less than the sum of the thicknesses of its component layers because each layer became thin owing to hot pressing.

Displacement measurement[40]

During testing, two gold disk electrodes were attached to an actuator strip with dimensions of 10 mm × 1 mm, and a triangular voltage was applied. The displacement between one side of the actuator and a location at a free length of 5 mm was measured using a laser-based displacement meter (Keyence, LC2100/2220). The actuator was activated using a waveform generator (Yokogawa Electric, FC 200) in conjunction with a potentio/galvanostat (Hokuto Denko, HA-501G), and its electrical parameters were measured. The resulting displacement, δ, could was then used to compute the strain difference between the bucky-gel electrode layers, ε, by assuming planar (*i.e.*, undistorted) cross sections along the actuator based on the following expression:

$$\varepsilon = 2d\delta/(L^2 + \delta^2). \quad (1)$$

Here, d is the actuator thickness, and L is the free length.[41]

Characterisation of the electrode and electrolyte

Cyclic voltammetry was performed using a two-electrode configuration and a potentiostat (Hokuto Denko, HSV-100) to estimate the double-layered capacitance of the polymer-supported bucky-gel electrode (at φ = 7 mm). These assessments were performed using the four-probe DC current method, which facilitates the evaluation of the electrical conductivities of the electrodes by measuring the voltage across the inner probe electrodes while applying a linear sweep wave of current. During these trials, a waveform generator (Yokogawa Electric, FC 200) was used in conjunction with a potentio/galvanostat (Hokuto Denko, HA-151) to obtain current–voltage plots. The conductivity of the gel electrolyte layer was assessed based on impedance measurements using a Solartron 1250 Impedance Analyzer. Stress–strain curves obtained using a thermal stress–strain instrument (Seiko, TMA/SS 6000) were employed to estimate the Young's moduli of the electrodes. Morphological differences in the electrode films were observed by acquiring FE-SEM images using a HITACHI S-5000 instrument.

Results and discussion

Table 1 presents the specific capacitance C (C_1 scaled by the weight of PEDOT:PSS, VGCFs) values obtained for different electrodes. The C values of the PEDOT:PSS/VGCF/EMI[BF_4]/EG electrodes were in the range 90–94 F g^{-1} (based on the weight of VGCFs) at a slow sweep rate of 1 mV s^{-1}. These values were significantly higher than those of the PEDOT:PSS/VGCF/EMI[BF_4] electrodes (70 F g^{-1}). The C values of the PEDOT:PSS/VGCF/EMI[CF_3SO_3]/EG electrodes (78–88 F g^{-1} based on the weight of VGCF), were also significantly higher than those of the PEDOT:PSS/VGCF/EMI[CF_3SO_3] electrodes (77 F g^{-1}). The C values of the PEDOT:PSS/VGCF/EMI[BF_4]/EG electrodes were also significantly higher than those of the PEDOT:PSS/VGCF/EMI[CF_3SO_3]/EG electrodes, therefore, the specific capacitance is dependent on IL anion species. This result can be attributed to the removal of insulating PSS from the surface of the PEDOT/PSS grains and crystallization of PEDOT, thus resulting in an increased specific capacitance of PEDOT:PSS/VGCF/IL/EG (Fig. 2).[22] The C values (based on the weight of PEDOT:PSS) of the PEDOT:PSS/VGCF/IL/EG electrodes showed a similar trend. The C values of the PEDOT:PSS/VGCF/EMI[BF_4]/EG electrodes were higher than those of the PEDOT:PSS/VGCF/EMI[CF_3SO_3]/EG electrodes. The specific capacitances of the PEDOT:PSS/VGCF/IL/EG electrodes can be attributed to the combination of the EDLC (*i.e.*, the VGCFs) and the FC (the PEDOT:PSS) mechanisms. The reversible oxidation and reduction reactions of PEDOT:PSS can be described as follows.[42–44] In addition, the reversible oxidation and reduction reactions (by electrons from electrode (VGCF)) of PEDOT:PSS and the EDLC mechanism can be expressed as follows.[45]

$$\text{PEDOT:PSS} + \delta\text{EMI}^+ + \delta e = (\text{PEDOT:PSS}^-)_\delta(\text{EMI}^+)_\delta + (1-\delta)\ \text{PEDOT:PSS}\ (0 < \delta < 1) \quad (2)$$

The electrical conductivities of electrode layers comprising PEDOT:PSS, VGCFs, EG, and an IL are summarized in Table 2. The PEDOT:PSS/VGCF/EMI[BF_4]/EG electrodes (14–22 cm^{-1}) have significantly higher conductivities than the PEDOT:PSS/VGCF/EMI[BF_4] electrodes (11 S cm^{-1}), thus suggesting that EG

Table 1 Effect of ethylene glycol on specific capacitance ($C = C_1$ divided by the weight of PEDOT:PSS or VGCFs) values (F g^{-1}) of PEDOT:PSS/VGCF/IL/EG electrodes and PEDOT:PSS/VGCF/IL electrodes (applied triangular voltage: ±0.5 V, sweep rate: 1 mV s^{-1})

IL		/PEDOT	/VGCF
EMI[BF_4]	EG 3%	51.5	89.8
	EG 30%	57.9	94.4
	EG 0%	41.9[a]	70.1[a]
EMI[CF_3SO_3]	EG 3%	52.8	78.2
	EG 30%	55.0	88.4
	EG 0%	49.4[a]	76.9[a]

[a] Ref. 39.

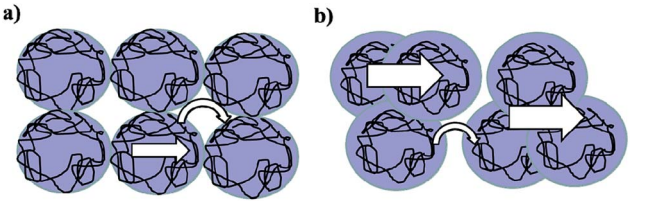

Fig. 2 Schematic representation of the electrical conduction mechanism of (a) PEDOT:PSS/VGCF/EMI[BF_4] and (b) PEDOT:PSS/VGCF/EMI[BF_4]/EG electrodes.

Table 2 Effect of ethylene glycol on the electrical conductivities (S cm^{-1}) of the PEDOT:PSS/VGCF/IL/EG electrodes

IL	EG 3%	EG 30%	EG 0%
EMI[BF_4]	14.0	22.0	10.6[a]
EMI[CF_3SO_3]	12.3	11.8	11.8[a]

[a] Ref. 39.

increased the conductivity. It is considered that PEDOT:PSS is actually a formation of 3-D crystal or a formation of parallel and linear structure formation.[19] The PEDOT:PSS/VGCF/EMI[BF_4]/EG electrodes have significantly higher conductivities than the PEDOT:PSS/VGCF/EMI[CF_3SO_3]/EG electrodes, therefore, the conductivity is dependent on IL anion species. This can be ascribed to the removal of insulating PSS from the surface of PEDOT/PSS grains and the crystallization of PEDOT, thus resulting in the formation of large numbers of highly conductive grains that improve charge carrier transport (Fig. 2).[22,46,47] However, the electrical conductivities of the PEDOT:PSS/VGCF/EMI[CF_3SO_3]/EG electrodes were similar to those of the PEDOT:PSS/VGCF/EMI[BF_4]/EG electrodes, which can be ascribed to the minimal effect of EG.

The measured strain values of the PEDOT:PSS/VGCF/IL/EG electrode and the PEDOT:PSS/VGCF/IL electrode using EMI [CF_3SO_3] as the IL are plotted against the frequency of the applied triangular voltage (±2 V) in Fig. 3. As the strain depends on the measurement frequency, the PEDOT:PSS/VGCF/IL/EG electrode and the PEDOT:PSS/VGCF/IL electrode using EMI [BF_4] show identical general trends. It can be observed that the strain of the PEDOT:PSS/VGCF/IL/EG actuator is similar to that of the PEDOT:PSS/VGCF/IL actuator across the frequency range of 0.05–100 Hz, while the strain of the PEDOT:PSS/VGCF/IL/EG actuator is larger than that of the PEDOT:PSS/VGCF/IL actuator across the frequency range of 0.005–0.05 Hz. It is considered that EG effects on the strain of the PEDOT:PSS/VGCF/IL actuator. This is because the *C* values of the PEDOT:PSS/VGCF/IL/EG electrodes were higher than those of the PEDOT:PSS/VGCF/IL electrodes across the frequency range of 0.005–0.05 Hz.

The maximum strain values of the four actuators using two different ILs are presented in Table 3. The strains of the PEDOT:PSS/VGCF/EMI[CF_3SO_3]/EG electrodes (1.18–1.28%) are 1.5–1.7 times greater than those of the PEDOT:PSS/VGCF/EMI [CF_3SO_3] electrodes (0.77%). Furthermore, the strains of the PEDOT:PSS/VGCF/EMI[BF_4]/EG electrodes are greater than those of the PEDOT:PSS/VGCF/EMI[BF_4] electrodes. The maximum strains of the PEDOT:PSS/VGCF/EMI[CF_3SO_3]/EG electrodes are greater than those of the PEDOT:PSS/VGCF/EMI [BF_4]/EG electrodes, therefore, the strain is dependent on IL anion species. Thus, both EDLC and FC mechanisms can be assumed to be responsible for the high specific capacitance of the PEDOT:PSS/VGCF/IL, with the latter mechanism being dominant. As noted above, the PEDOT:PSS polymer in the PEDOT:PSS/VGCF/IL actuator plays two roles (the base polymer and the FC electrode), thus allowing the device to generate strain that is useful for real-world applications. The result can be attributed to the removal of insulating PSS from the surface of the PEDOT/PSS grains and the crystallization of PEDOT, thus leading to an increase in the specific capacitances of the PEDOT:PSS/VGCF/IL/EG across the frequency range of 0.005–0.05 Hz.[22]

The stress–strain curve for the PEDOT:PSS/VGCF/EMI[BF_4]/EG 30% and PEDOT:PSS/VGCF/EMI[BF_4] electrodes are shown in Fig. S1.† It is considered that there is effect of EG.[46] The Young's moduli of the PEDOT:PSS/VGCF/IL/EG electrodes were similar to those of the PEDOT:PSS/VGCF/IL electrodes (Table 4).

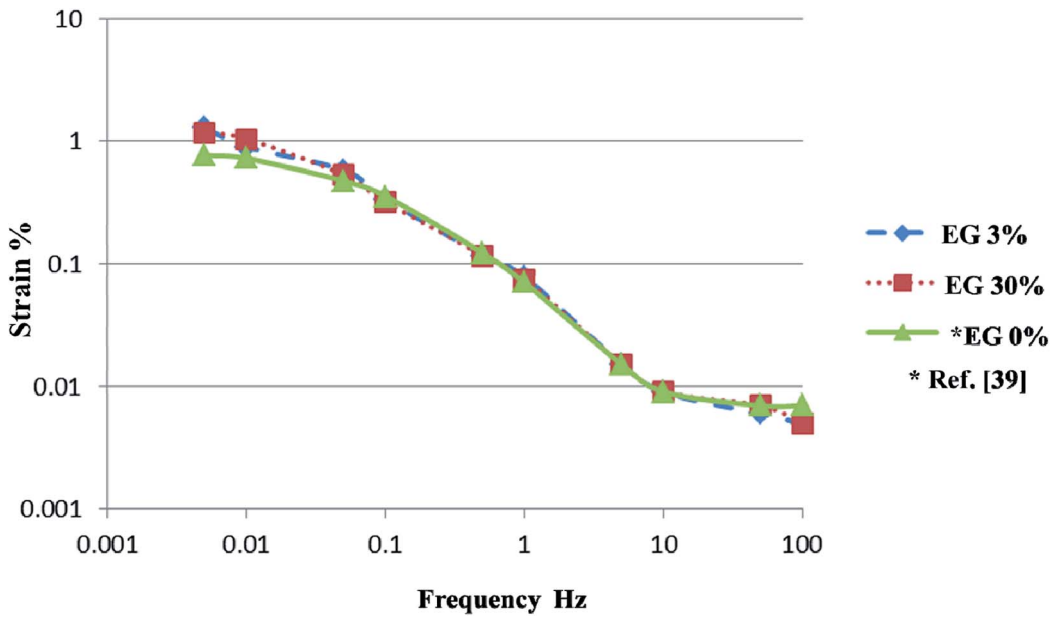

Fig. 3 Strain values (ε%) calculated from the peak-to-peak displacements of the PEDOT:PSS/VGCF/IL/EG and PEDOT:PSS/VGCF/IL electrode actuators as functions of applied triangular voltage (±2 V) frequency. IL: EMI[CF_3SO_3].

Table 3 Effect of ethylene glycol on the maximum strain (%) values of the PEDOT:PSS/VGCF/IL/EG electrodes

IL	EG 3%	EG 30%	EG 0%
EMI[BF_4]	0.94	0.84	0.79[a]
EMI[CF_3SO_3]	1.28	1.18	0.77[a]

[a] Ref. 39.

The result can be ascribed to small effect of EG. Furthermore, scanning electron microscopy (SEM) micrographs (magnification: 300000×) of (a) PEDOT:PSS/VGCF/EMI[BF_4] and (b) PEDOT:PSS/VGCF/EMI[BF_4]/EG electrodes is shown in Fig. 4. These results suggest that a network of open mesopores is formed in the electrodes by highly entangled VGCFs.[34]

Finally, the maximum stress values (σ) generated during actuation were calculated according to Hooke's law ($\sigma = Y \times \varepsilon_{max}$) using the values of maximum strain (ε_{max}) and Young's modulus (Y) (Table 5).

The σ values of the PEDOT:PSS/VGCF/EMI[CF_3SO_3]/EG actuators were greater than those of the PEDOT:PSS/VGCF/EMI[BF_4]/EG actuators, therefore, the σ value is dependent on IL anion species. The two σ values of the PEDOT:PSS/VGCF/EMI[CF_3SO_3]/EG actuators were ~1.6 to ~1.8 times greater than those of the PEDOT:PSS/VGCF/EMI[CF_3SO_3] actuators. Thus, the PEDOT:PSS/VGCF/IL actuators could generate the maximum stress values suitable for real-world applications, such as tactile displays.

Table 4 Effect of ethylene glycol on the Young's moduli (MPa) of the PEDOT:PSS/VGCF/IL/EG electrodes

IL	EG 3%	EG 30%	EG 0%
EMI[BF_4]	202	192	203[a]
EMI[CF_3SO_3]	190	184	181[a]

[a] Ref. 39.

Previously, we proposed a mechanism for the bending of a conventional PVdF(HFP)/SWCNT/IL actuator, according to which the application of voltage between the two electrode layers leads to the transfer of cations and anions from the gel electrolyte layer to the cathode and anode layers, respectively. This results in the formation of an electric double layer with negatively and positively charged nanotubes; the associated ion transport causes the cathode layer to swell and the anode layer to shrink.[27,33,48] Furthermore, in the present work, the anode layer swelled and expanded owing to ion migration. Therefore, we propose that the swelling and expansion of the anode layer according to the FC mechanism along with the EDLC mechanism contribute to actuator motion at low frequencies. In other words, ion transport causes the cathode layer to swell in addition to causing the anode layer to shrink. Therefore, the actuator bends toward the anode side (Fig. S2†).

In a previous study,[22] ILs performed very well as permanent conductivity enhancers in PEDOT:PSS films. EG helps with the formation of three-dimensional conducting networks between smaller PEDOT:PSS domains owing to the removal of insulating PSS from the surface of the PEDOT/PSS grains and crystallization of PEDOT, thus resulting in increased specific capacitances of the PEDOT:PSS/VGCF/IL/EG electrode (Fig. 2). Based on these results, the PEDOT:PSS/VGCF/IL/EG electrodes were observed to have higher C values than the PEDOT:PSS/VGCF/IL electrodes in the low frequency range of 0.005–0.05 Hz.

In a previous study,[28] we investigated the voltage–current and voltage–displacement characteristics of a bucky-gel actuator under the application of a triangular waveform voltage to the device at various frequencies. We proposed an electrochemical equivalent circuit model to quantitatively describe the frequency dependence of the generated strain. This model, comprising the combined resistance and capacitance of the electrode layer and the combined resistance of the electrolyte layer, allowed us to predict the time constant of the response and the low-frequency limit of the strain. In the present study, a similar double-layer charging kinetic model with the EDLC and FC mechanisms has been employed to successfully predict variations in the frequency-dependent displacement in the case

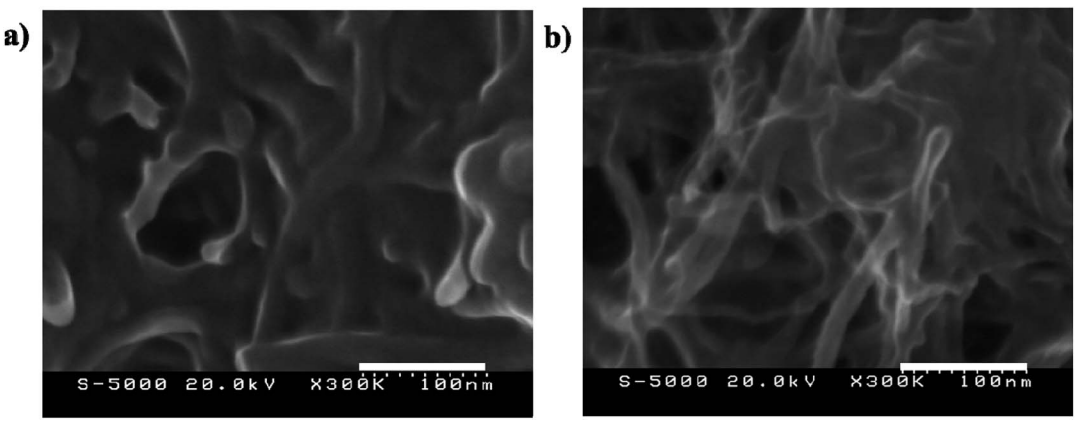

Fig. 4 Scanning electron microscopy (SEM) micrographs (magnification: 300000×) of (a) PEDOT:PSS/VGCF/EMI[BF_4] and (b) PEDOT:PSS/VGCF/EMI[BF_4]/EG electrodes.

Table 5 Effect of ethylene glycol for maximum generated stress values (MPa) for PEDOT:PSS/VGCF/IL/EG electrodes

IL	EG 3%	EG 30%	EG 0%
EMI[BF_4]	1.90	1.61	1.60[a]
EMI[CF_3SO_3]	2.43	2.17	1.39[a]

[a] Ref. 39.

of the PEDOT:PSS/VGCF/IL/EG electrode actuators (see ESI† for details).

Conclusions

We developed a novel actuator (PEDOT/VGCF/IL/EG), which exhibited a superior performance compared to PEDOT/VGCF/IL devices. The maximum strain and maximum generated stress of the PEDOT:PSS/VGCF/IL/EG actuators were considerably higher than those of the PEDOT:PSS/VGCF/IL actuators because of the use of EG. EG helps to form three-dimensional conducting networks between small PEDOT:PSS domains. This can be ascribed to the removal of insulating PSS from the surface of the PEDOT/PSS grains and crystallization of PEDOT. EG helps to increase the specific capacitance, strain, and maximum generated stress values relative to those obtained for PEDOT:PSS/VGCF/IL actuators. Similar to the case of the PEDOT:PSS/VGCF/IL actuators, variation in the displacement of the frequency of the PEDOT:PSS/VGCF/IL/EG actuators could be modeled using an equivalent circuit comprising ionic resistance, double-layer and faradaic capacitance, and electrode resistance in series.

The flexible and robust films using the effects of EG combined with PEDOT:PSS/VGCF/IL presented in this work are promising for their applications as electrode materials in wearable energy conversion devices. The same concept can be employed to develop other PEDOT-based electrochemical materials for their use in energy conversion applications.

Conflicts of interest

There are no conflicts to declare.

Acknowledgements

This work was partly supported by the KAKENHI Grant-in Aid for Scientific Research Council from the Japan Society for the Promotion of Science (JSPS).

Notes and references

1 K. R. Prasad, K. Koga and N. Miura, *Chem. Mater.*, 2004, **16**, 1845–1847.
2 M. Kalaji, P. J. Murphy and G. O. Williams, *Synth. Met.*, 1999, **102**, 1360–1361.
3 Y. Zhou, B. He, W. Zhou, J. Huang, X. Li, B. Wu and H. Li, *Electrochim. Acta*, 2004, **49**, 257–262.
4 V. Gupta and N. Miura, *Mater. Lett.*, 2006, **60**, 1466–1469.
5 L. Fan and J. Maier, *Electrochem. Commun.*, 2006, **8**, 937–940.
6 A. Elschner, S. Kirchmeyer, W. Lövenich, U. Merker and K. Reuter, *PEDOT: Principles and Applications of an Intrinsically Conductive Polymer*, CRC Press: Taylor & Francis Group, Boca Raton, London, New York, 2011, vol. 10.
7 J. Zhou, D. H. Anjum, G. Lubineau, E. Q. Li and S. T. Thoroddsen, *Macromolecules*, 2015, **48**, 5688–5696.
8 J. Zhou, E. Q. Li, R. Li, X. Xu, I. A. Ventura, A. Moussawi, D. H. Anjum, M. N. Hedhili, D.-M. Smilgies, G. Lubineau and S. T. Thoroddsen, *J. Mater. Chem. C*, 2015, **3**, 2528–2538.
9 A. G. MacDiarmid, *Angew. Chem., Int. Ed.*, 2001, **40**, 2581–2590.
10 D. Hohnholz, H. Okuzaki and A. G. MacDiarmid, *Adv. Funct. Mater.*, 2005, **15**, 51–56.
11 H. Sirringhaus, T. Kawase, R. H. Friend, T. Shimoda, M. Inbasekaran, W. Wu and E. P. Woo, *Science*, 2000, **290**, 2123–2126.
12 H. Okuzaki, Y. Harashina and H. Yan, *Eur. Polym. J.*, 2009, **45**, 256–261.
13 R. K. Cheedarala, J.-H. Jeon, C.-D. Kee and I.-K. Oh, *Adv. Funct. Mater.*, 2014, **24**, 6005–6015.
14 S.-S. Kim, J.-H. Jeon, H. I. Kim, C.-D. Kee and I.-K. Oh, *Adv. Funct. Mater.*, 2015, **25**, 3560–3570.
15 M. Kotal, J. Kim, K. J. Kim and I.-K. Oh, *Adv. Mater.*, 2016, **28**, 1610–1615.
16 J. Zhou, T. Furukawa, H. Shirai and M. Kimura, *Macromol. Mater. Eng.*, 2010, **295**, 671–675.
17 J. Zhou, M. Mulle, Y. Zhang, X. Xu, E. Q. Li, F. Han, S. T. Thoroddsen and G. Lubineau, *J. Mater. Chem. C*, 2016, **4**, 1238–1249.
18 J. Ouyang, C.-W. Chu, F.-C. Chen, Q. Xu and Y. Yang, *Adv. Funct. Mater.*, 2005, **15**, 203–208.
19 J. Ouyang, Q. Xu, C.-W. Chu, Y. Yang, G. Li and J. Shinar, *Polymer*, 2004, **45**, 8443–8450.
20 J. S. K. M. Jönsson, J. Birgerson, X. Crispin, G. Greczynski and W. Osikowicz, *Synth. Met.*, 2013, **139**, 1–10.
21 X. Crispin, F. L. E. Jakobsson, A. Crispin, P. C. M. Grim, P. Andersson, A. Volodin, C. van Haesendonck, M. van der Auweraer, W. R. Salaneck and M. Berggren, *Chem. Mater.*, 2006, **18**, 4354–4360.
22 H. Okuzaki, Y. Harashina and H. Yan, *Eur. Polym. J.*, 2009, **45**, 256–261.
23 *Directions for development of the field of Electroactive Polymer (EAP)*, ed. Y. Bar-Cohen, SPIE Press, Washington, DC, 2011.
24 E. Smela, *Adv. Mater.*, 2003, **15**, 481–494.
25 M. Shahinpoor, *Electrochim. Acta*, 2003, **48**, 2343–2353.
26 T. Fukushima, K. Asaka, A. Kosaka and T. Aida, *Angew. Chem., Int. Ed.*, 2005, **44**, 2410–2413.
27 K. Mukai, K. Asaka, K. Kiyohara, T. Sugino, I. Takeuchi, T. Fukushima and T. Aida, *Electrochim. Acta*, 2008, **53**, 5555–5562.
28 I. Takeuchi, K. Asaka, K. Kiyohara, T. Sugino, K. Mukai, T. Fukushima and T. Aida, *Electrochim. Acta*, 2009, **53**, 1762–1768.
29 T. Fukushima, A. Kosaka, Y. Ishimura, T. Yamamoto, T. Takigawa, N. Ishii and T. Aida, *Science*, 2003, **300**, 2072–2074.

30 W. Lu, A. G. Fadeev, B. Qi, E. Smela, B. R. Mattes, J. Ding, G. M. Spinks, J. Mazurkiewicz, D. Zhou, G. G. Wallace, D. R. MacFarlane, S. A. Forsyth and M. Forsyth, *Science*, 2002, **297**, 983–987.
31 N. Terasawa, I. Takeuchi and H. Matsumoto, *Sens. Actuators, B*, 2009, **139**, 624–630.
32 N. Terasawa, I. Takeuchi, H. Matsumoto, K. Mukai and K. Asaka, *Sens. Actuators, B*, 2011, **156**, 539–545.
33 I. Takeuchi, K. Asaka, K. Kiyohara, T. Sugino, N. Terasawa, K. Mukai and S. Shiraishi, *Carbon*, 2009, **47**, 1373–1380.
34 N. Terasawa, N. Ono, Y. Hayakawa, K. Mukai, T. Koga, H. Higashi and K. Asaka, *Sens. Actuators, B*, 2011, **160**, 161–167.
35 B. Babakhani, *Electrochim. Acta*, 2010, **55**, 4014–4024.
36 S. Sarangapani and B. V. Tilak, *J. Electrochem. Soc.*, 1996, **143**, 3791–3799.
37 G. Wang, L. Zhang and J. Zhang, *Chem. Soc. Rev.*, 2012, **41**, 797–828.
38 N. Terasawa and K. Asaka, *Langmuir*, 2016, **32**, 7210–7218.
39 N. Terasawa and K. Asaka, *Sens. Actuators, B*, 2017, **248**, 273–279.
40 N. Terasawa and I. Takeuchi, *Sens. Actuators, B*, 2010, **145**, 775–780.
41 Q. Pei and O. Inganas, *J. Phys. Chem.*, 1992, **96**, 10507–10514.
42 J. P. Zheng and T. R. Jow, *J. Electrochem. Soc.*, 1995, **142**, L6–L8.
43 H. Okuzaki, S. Takagi, F. Hishiki and R. Tanigawa, *Sens. Actuators, B*, 2014, **194**, 59–63.
44 M. Dietrich, J. Heinze, G. Heywang and F. Jonas, *J. Electroanal. Chem.*, 1994, **369**, 87–92.
45 T. F. Otero, J. G. Martinez and J. Arias-Pardilla, *Electrochim. Acta*, 2012, **84**, 112–128.
46 M. G. Tadesse, C. Loghin, Y. Chen, L. Wang, D. Catalin and V. Nierstrasz, *Smart Mater. Struct.*, 2017, **26**, 065016.
47 M. Döbbelin, R. Marcilla, M. Salsamendi, C. Pozo-Gonzalo, P. M. Carrasco, J. A. Pomposo and D. Mecerreyes, *Chem. Mater.*, 2007, **19**, 2147–2149.
48 N. Terasawa and I. Takeuchi, *Electrochim. Acta*, 2014, **123**, 340–345.